Ceramics International 50 (2024) 37430–37440

Contents lists available at ScienceDirect

Ceramics International

journal homepage: www.elsevier.com/locate/ceramint

Sintering activation energies of anisotropic layered and particle alumina/zirconia-based composites and their mechanical response

Daniel Drdlik [a,b], Ilya Sokolov [a], Hynek Hadraba [c], Zdenek Chlup [c], Katarina Drdlikova [a], Karel Maca [a,b,*]

[a] CEITEC BUT, Brno University of Technology, Purkynova 123, 612 00, Brno, Czech Republic
[b] Institute of Materials Science and Engineering, Brno University of Technology, Technicka 2, 616 00, Brno, Czech Republic
[c] Institute of Physics of Materials of the Czech Academy of Sciences, Zizkova 22, 616 00, Brno, Czech Republic

ARTICLE INFO

Handling Editor: Dr P. Vincenzini

Keywords:
Sintering
Activation energy
High-temperature dilatometry
Laminate
Particle composite

ABSTRACT

Information on the sintering activation energy is currently focused on evaluation of single-phase ceramic systems. This work shows the results of high-temperature dilatometry measurements of layered and particle composites based on alumina and zirconia. Layered composites with different layer thickness ratios and particle composites with variable composition in the entire concentration range were prepared by electrophoretic deposition allowing manufacturing composites with precious design and strongly bonded interfaces. The phenomena observed during the high-temperature dilatometry measurements are discussed, and the data were used to calculate the sintering activation energies of composites using the modified Master Sintering Curve concept. By covering a wide range of composite designs, it was possible to determine differences in activation energies and to show their dependence on the direction in the case of laminate composites given by the directionally dependent sintering behaviour. Sintering activation energies of layered composites were always higher than for monoliths due to constrained sintering showing maximum sintering activation energies at lower volumes of zirconia in the layers for longitudinal and transversal orientation of the samples. A similar trend was identified in particle composites due to slowed down alumina densification by the pinning effect. Additionally, mechanical properties represented by Vickers hardness and indentation elastic modulus were related to the microstructure developed during sintering. The effects of interconnectivity of phases present in the composites together with other parameters of the microstructure were described.

1. Introduction

Generally, sintering is the densification of free powder or powder compact at a temperature below the material's melting point. Such a thermally driven process has been known for thousands of years; however, in the last century, considerable efforts have been made in the development of sintering methods and the sintering of various advanced ceramic materials. Along with this, various sintering models were derived, which are subject to constant refinement. One of the significant parameters allowing a better insight into the physical background of the sintering is the activation energy of sintering also referred to as apparent activation energy.

The beginnings of the study of the sintering activation energy are related to the work of Young and Cutler [1] who studied the densification of alumina, zirconia and titania at constant rates of heating to describe solid-solid reactions. Their work was followed up by Wang and Raj [2,3] who used constant-heating-rate experiments to estimate activation energy in alumina, alumina/titania and alumina/zirconia particle composites. Since then, many scientific works have been published reporting the sintering activation energies of various ceramics. Afterwards, an engineering tool based on non-isothermal sintering for predicting the sintering process and also determining sintering activation energies was developed [4].

Su and Johnson [4] developed the concept of master sintering curve (MSC) assuming that the geometric parameters related to the sintering are functions only of green body microstructure (and therefore independent on the heating profile) and that only one prevalent diffusion mechanism is dominant in the sintering process. The MSC gives the relation between the thermal history of the sintering (using the parameter Q describing the activation energy of sintering) and density.

* Corresponding author. CEITEC BUT, Brno University of Technology, Purkynova 123, 612 00, Brno, Czech Republic.
E-mail address: maca@fme.vutbr.cz (K. Maca).

https://doi.org/10.1016/j.ceramint.2024.04.263
Received 31 January 2024; Received in revised form 28 March 2024; Accepted 20 April 2024
Available online 22 April 2024

The experimental approach of the concept is based on the time-consuming mathematical iterations drawing data from the number of sintering experiments conducted at different heating regimes. However, the following works brought simplification in the construction of the MSC using computer programs [5] together with dilatometric data [6,7] reducing computing time dramatically.

A lot of works have been published up to now to establish activation energies of monolithic ceramics. The most attention was paid to alumina [1–3,7–13], zirconia [3,7,9,14–16], silicon nitride [17], zinc oxide [8], uranium dioxide [18,19], yttrium oxide [20], etc. Moreover, it was found that the sintering technique can also play a role in diffusion mechanisms in studied materials affecting the activation energy of sintering [8]. Therefore, not only conventional sintering [1–3,7–9] but also microwave sintering [8], sintering in microwave-induced oxygen plasma [21], spark plasma sintering [22], and liquid phase sintering [17] were considered to report complex data concerning activation energy of sintering at different conditions.

However, a more complex situation arises when multiple phases appear in the material. The volume of these phases can be distributed in an ordered manner in the form of individual particles (grains) or layers. The sintering activation energy of the particle composites based on alumina and zirconia ceramics was studied for the very first time by Wang and Raj [2,3]. They showed that the activation energy remains in the range of 700 ± 100 kJ/mol when the composition changes from 5 to 95 vol% zirconia [3]. Although the authors reported full range composition, only concentrations of 0, 5, 50, 95 and 100 vol% zirconia were investigated. Therefore, a substantial part of the concentration profile of this ceramic particle composite is missing. Even less data is known about layered materials. Maca et al. [9] recently showed layered composites where alternating layers with different thicknesses and/or volumes of alumina and zirconia were evaluated in terms of sintering activation energies. The original MSC works with the density of sintered bodies and assumes that their sintering shrinkage is isotropic [4]. For non-isotropic shrinkage, the MSC concept had to be modified to the so-called Master Shrinkage Curve [9].

Moreover, it was found that strongly bonded layers exhibit sintering anisotropy demonstrated by different sintering activation energies in the two measurement directions of the sintered samples. However, as with particle composites [3], only a small concentration range was studied in this work, i.e., the composite that had 50 vol% represented by layers of alumina and the rest by zirconia. Thus, a much more precise insight into this issue is necessary for a better understanding of the sintering process in particle and layered ceramics.

These materials are very interesting from the point of view of their microstructural and mechanical properties. The alumina and zirconia particle composites can be divided into two categories depending on the major phase on Zirconia Toughened Alumina (ZTA, alumina is a major phase) and Alumina Toughened Zirconia (ATZ, zirconia is a major phase) providing improved strength, fracture resistance, elasticity, hardness, toughness, and/or wear resistance etc. These composites are widely employed in various structural applications across different industries such as cutting tools [23–25], aerospace applications [26], electrical insulators [27], wear-resistant products (nozzles, pump parts, valves etc.) [28], dental implants [29,30], orthopaedic replacements [31,32], coatings [29,33] etc. Layered architectures which are composed of alternating layers of two or more different ceramic materials, offer unique fracture behaviour if the internal stresses are generated in the layers during sintering and cooling. In the case of alumina/zirconia layered material, the internals stresses arise during densification of the composite at the heating stage and dwell time on the sintering temperature [34]. However, such internal stresses are relatively small and can relax during the dwell time at the sintering temperature via the diffusion processes. More significant are internal stresses developed when reference (stress-free) temperature is exceeded [35] at the cooling stage of sintering. The stresses inside the strongly bonded layered structure originate from the thermal expansion mismatch of the ceramic materials resulting, among others, in a crack deflection behaviour [36]. Moreover, the presence of zirconia might originate transformation toughening mechanisms, which operate at the microstructural level [37].

The paper substantially expands the existing knowledge about the sintering activation energy of the particle and layered structures that are composed of alumina and zirconia in the full volume (concentration) range. This is achieved by using a modified MSC concept and high-temperature dilatometry. The sintering behaviour is correlated with the mechanical response of composite materials and discussed.

2. Experimental

Alumina (HP-DBM, Malakoff Ind., USA) and 3 mol.% yttria stabilised zirconia (TZ-3YS-E, Tosoh, Japan) ceramic powders with mean particle sizes of 0.47 and 0.14 μm, respectively, were used for this study. The single-phase nature of as-received powders is demonstrated in Fig. 1. The phase composition of as-received powders was analysed by X-ray powder diffractometer SmartLab 3 kW (XRD, Rigaku, Japan) with Bragg-Brentano setup and Cu-Kα radiation source (λ = 1.54 Å). The powders were dispersed in colloidal suspensions for their wet shaping via electrophoretic deposition (EPD). To this purpose, the suspensions were composed of 15 wt% alumina and/or zirconia, 12.75 wt% monochloroacetic acid (99 %, Merck, Germany) acting as a stabiliser, and 2-propanol dispersant (p.a., Lachner, Czech Republic) in the amount of 72.25 wt%. Suspensions were stirred mechanically in an ultrasonic bath (output power 320 W) for 30 min prior to EPD.

The vertical position of two stainless steel electrodes with an effective surface area of 18.2 cm^2 placed at a distance of 26 mm between them was used for EPD in a glass cell. The electrodes connected with a stabilised source allowed to set a circuit with a constant current of 5 mA. Three types of ceramic materials were prepared i) monoliths (standards – alumina or zirconia denoted as A and Z) ii) particle composites (i.e., homogeneous mixture of alumina and zirconia with given volume fraction), and iii) layered composites (i.e., alternating alumina and zirconia layers with various thickness). The particle composites (denoted as PC) were prepared by mixing of certain volume fraction of zirconia (i.e., 17, 25, 33, 45, 50, 55, 66, 75, and 83 vol%) into alumina. The depositions lasting 30 min were interrupted each 5 min and the suspensions were thoroughly stirred to prevent sedimentation of the particles. Based on our previous results [38,39] concerning deposition kinetic studies of alumina and zirconia we were able to fabricate layered structures (laminates; denoted as LC) with a precise thickness of layers. The laminates were designed with the same volume fractions of alumina and zirconia as in particle composites and the desired concentrations

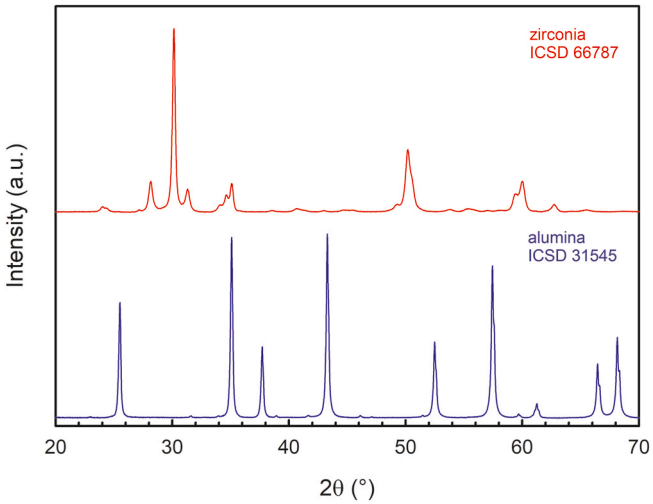

Fig. 1. XRD patterns of alumina and zirconia as received powders.

were set by different layers thickness ratios. The thickness ratios (A:Z) of 5:1, 3:1, 1.2:1 and vice versa were prepared by the repeated moving of deposition electrode from suspension containing alumina to zirconia suspension at strictly defined time segments. The total number of layers was set to 100. The information about prepared samples including volume fractions of ceramic materials is summarised in Table 1. The deposits were dried at room temperature for 24 h after deposition. Subsequently, they were removed from deposition electrodes and annealed at 800 °C for 1 h in an ambient atmosphere.

The prepared samples were cut out from the green bodies in longitudinal (perpendicular to the deposition direction) and transversal orientation (parallel to the deposition direction) in the form of bars (4 × 4 × 10 mm) or cylinders (ø5 × ca 5 mm), respectively. For a better illustration of the mentioned orientations, Fig. 2 shows a scheme of a deposition electrode with layered structure. The samples underwent high-temperature dilatometry sintering using L70/1700 (Linseis, Germany) at 1500 °C with heating rates 2, 5, 10, and 20 °C/min for 2 h at sintering temperature. The samples intended for mechanical testing were sintered in a conventional furnace at 1500 °C with a heating rate of 10 °C/min and a dwell time of 2 h.

The coefficient of thermal expansion was calculated using Equation (1):

$$\alpha = \frac{\varepsilon_{T\ room} - \varepsilon_{T\ max}}{(T_{room} - T_{max}) \bullet 100}, \quad (1)$$

where $\varepsilon_{T\ room}$ is the shrinkage after cooling, ε_{max} is the shrinkage at the end of the dwell, T_{room} is the temperature after cooling, and T_{max} is the dwell temperature.

The sintering shrinkage was calculated using Equation (2):

$$\varepsilon(t,T) = \varepsilon_{instant}(t,T) - \alpha \bullet 100 \bullet (T - T_{room}), \quad (2)$$

where $\varepsilon_{instant}(t,T)$ is the instantaneous measured shrinkage, t is the time, and T is the actual temperature.

To examine activation energies, allowing deeper insight into the physical background of the sintering process of anisotropic layered and particle composites, the modified Master Sintering Curve model [9] was applied for the construction of Master Shrinkage Curves. Assuming the work of Hansen et al. [40], it includes the relationship between the thermal history of the sintering and linear shrinkage under the following Equation (2):

Table 1
Summarization of sample's compositions and their microstructural properties.

Sample	Z content (vol%)	A/Z thickness ratio	green density (% t.h.)	final density (% t.h.)	A/Z grain size (μm/μm)
monoliths					
A	0	–	61.0	98.3	1.3/-
Z	100	–	47.4	99.7	-/0.3
particle composites					
PC17	17	–	57.6	97.7	1.0/0.5
PC25	25	–	56.4	97.9	0.9/0.5
PC33	33	–	55.6	98.1	0.8/0.5
PC45	45	–	53.4	98.4	0.7/0.4
PC50	50	–	53.1	98.6	0.7/0.5
PC55	55	–	53.1	99.0	0.7/0.5
PC66	66	–	51.1	99.2	0.7/0.5
PC75	75	–	51.0	99.5	0.6/0.5
PC83	83	–	50.6	99.8	0.6/0.5
layered composites – longitudinal orientation					
LC17	17	5:1	58.1	97.6	1.6/0.6
LC25	25	3:1	57.1	98.7	1.7/0.6
LC45	45	1.2:1	54.8	98.6	1.8/0.6
LC55	55	1:1.2	54.7	99.9	1.6/0.6
LC75	75	1:3	51.1	99.6	1.5/0.6
LC83	83	1:5	50.4	99.9	1.5/0.6

A, Z – Alumina, Zirconia; PC – Particle Composite; LC – Layered Composite. Sintering regime 1500 °C/2h; heating rate of 10 °C/min.

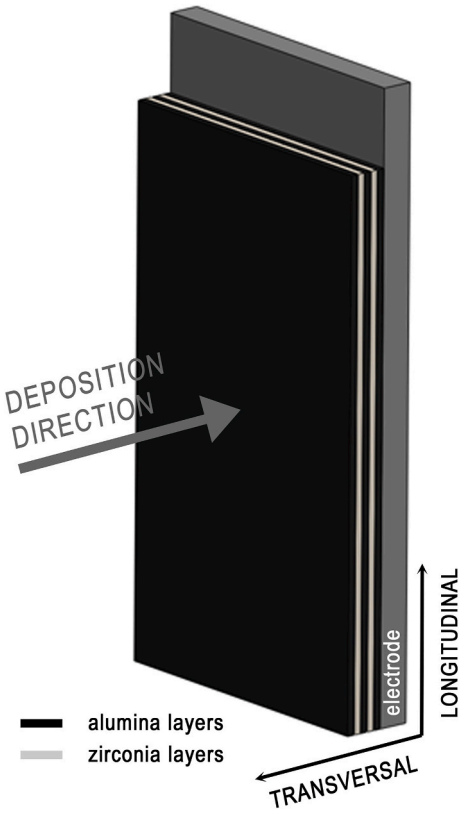

Fig. 2. Scheme of a deposition electrode with layered structure.

$$\frac{-k}{\gamma \Omega D_0} \int_0^{\varepsilon_f} \frac{(G(\varepsilon))^n}{\Gamma(\varepsilon)} d\varepsilon = \Theta = \int_0^t \frac{1}{T} \exp\left(-\frac{Q}{RT}\right) dt, \quad (3)$$

where function Θ describes the thermal history of the sintering with the activation energy of sintering Q, k is the Boltzmann constant, γ is the surface energy, Ω is the atomic volume, D_0 is the coefficient of a diffusion process, G is the mean grain size, Γ represents scaling parameters, ε is the linear shrinkage, T is the thermodynamic temperature, R is the gas constant and t is the time. The four heating regimes were conducted for all samples to obtain sufficient data sets to find the best overlap of individual curves calculated using Eq. (1). The criterion of Mean Perpendicular Curve Distance was used to find the best overlap [41].

The densities of the green bodies and sintered samples were measured using the soaking method and Archimedes principle. The microstructure of the samples was observed using scanning electron microscopy Verios 460L (SEM, FEI, Czech Republic). The mean grain size (MGS) was determined using the linear intercept method from at least 5 images and the results were multiplied by a correction factor of 1.56 [42].

Cooling from the sintering temperature can cause the development of internal stresses as was mentioned in the introduction chapter. The theoretically estimated internal stresses for laminate based on the volume fraction of individual phases independent of the layer design are shown in Fig. 3a) [43]. The input values for internal stress calculation were taken from our previous works [35,44]. Similarly to laminates, the internal stresses are also developed in the particle composite materials due to CTE mismatch and can influence hardness, modulus and/or strength in the dependence of design and phase volume fraction. In the particle composite, the level of internal stresses within individual phases is estimated by Eshelby's inclusion model in the dependence on the volume fraction, see Fig. 3b) [45,46]. The model estimates stresses based on the fact of which phase forms the matrix (σ_m) and which

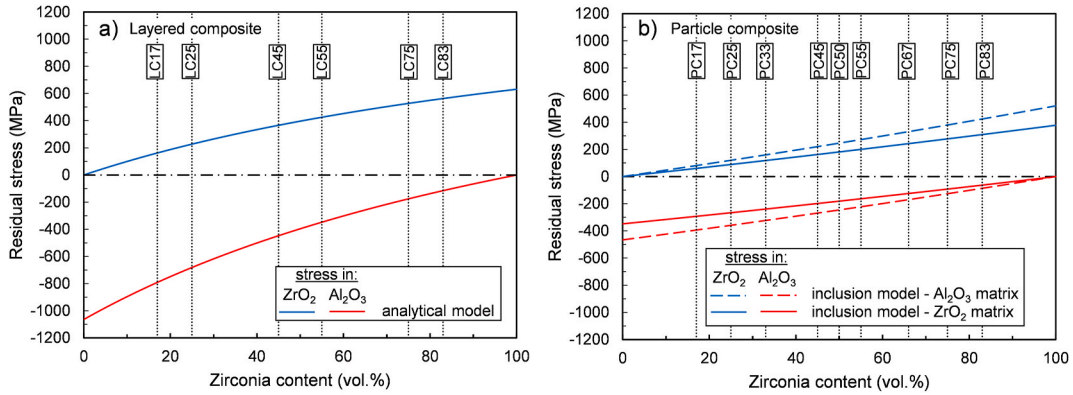

Fig. 3. Theoretically estimated internal stresses developed due to thermal expansion mismatch for each phase in a) laminates and b) particle composites with two limit situations, i.e. upper and lower bounds for each phase. LC – Layered Composite, PC – Particle Composite.

reinforcement (σ_f).

$$\sigma_f = \frac{-2E_m(1-v_f)\beta\alpha^*}{A}, \tag{4}$$

$$\sigma_m = \frac{2E_m v_f \beta\alpha^*}{A}, \tag{5}$$

$$A = (1-v_f)(\beta+2)(1+\mu_m) + 3\beta v_f(1-\mu_m), \tag{6}$$

$$\beta = \frac{E_f(1+\mu_m)}{E_m(1-2\mu_f)}, \tag{7}$$

$$\alpha = (\alpha_f - \alpha_m)\Delta T, \tag{8}$$

where $\Delta T = T - T_{room}$ similarly as in Equation (1), v, E, μ *and* α are the volume fraction, elastic modulus, Poisson's ratio and CTE for given phase, indexes *m* and *f* mean matrix or reinforcement, respectively.

The microhardness of the particle composites was measured on the polished cross-section surfaces using an instrumented Vickers indentation technique using an electromechanical machine Z2.5 equipped with a ZHU0.2 indentation head (Zwick/Roell, Germany). The indentation load of 5 kg (~49 N) was selected to incorporate into the indentation imprint a significant number of grains to sufficiently describe the mechanical behaviour of particle composite (i.e., compare imprint diagonals of 70–80 μm vs 0.5–1.0 μm grain size). The instrumented indentation was used to estimate the indentation elastic modulus calculated from the unloading part of the recorded loading curve.

Experimental data used for this paper are available in a general-purpose open repository [47], Zenodo, developed under the European OpenAIRE program and operated by CERN.

3. Results and discussion

The alumina and zirconia green bodies prepared by EPD reached the relative density of 61.0 % and 47.4 % t.d., respectively (see Table 1). One could expect that the layered or particle materials composed from these ceramics using the same fabrication technique should follow the superposition of alumina and zirconia densities. This assumption is confirmed in Fig. 4 showing relative densities of annealed layered composites and particle composites prepared by EPD. Newly acquired data was supplemented with information from recently published results (red symbols) [9]. The linear dependence of measured values is visible for both types of composites. Moreover, the recently published values fit very well the trend of the newly acquired data demonstrating good reproducibility of the experiment. The EPD shaping technique makes it possible to obtain composites, whether they are made up of bulk layers or dispersed particles, which have the same density for individual material compositions.

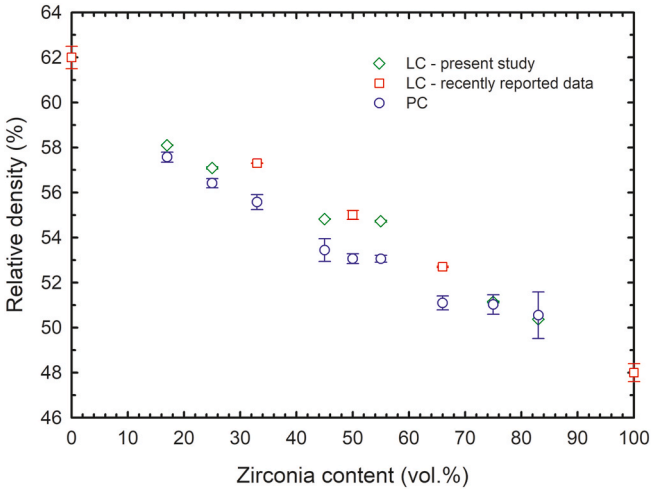

Fig. 4. Dependence of relative density on zirconia content in monoliths, layered and particle composites in their green state (red symbols – reported data from Maca et al. [9]). LC – Layered Composite, PC – Particle Composite. (For interpretation of the references to colour in this figure legend, the reader is referred to the Web version of this article.)

The lower green density of the zirconia monolith resulted in higher shrinkage in the longitudinal and transversal orientation of the measured sample during sintering than that of the alumina. This is documented in Fig. 5 where the sintering shrinkage and sintering shrinkage rate of monoliths and layered composites in longitudinal and transversal orientations are given. Alumina and zirconia shrinkage in longitudinal and transversal orientation shows sintering shrinkage anisotropy. Fig. 5a and b shows that the total difference in sintering shrinkage in longitudinal and transversal orientations for alumina was 4.8 % (ε_L = 13.1 % vs. ε_T = 17.9 %) whereas for zirconia it was 1.9 % (ε_L = 22.3 % vs. ε_T = 24.2 %). The origin of the anisotropy can be found in the anisotropic (oval) shape of alumina particles contrary to more less spherical shape of zirconia particles [38] resulting in shape-oriented packing of charged particles in an electrical field during EPD [48].

The sintering shrinkage curves of layered samples in longitudinal orientation (see Fig. 5a) are more inclined to the shrinkage curve of alumina monolith even when a high volume of zirconia is present in the layers, e.g. see sample LC83. It means, that the sintering in longitudinal orientation is more controlled by the alumina than zirconia content in layered structures. To explain this behaviour, the initial particle size must be considered. Zirconia layers composed of smaller particles tend to shrink earlier than alumina layers because the sintering temperature

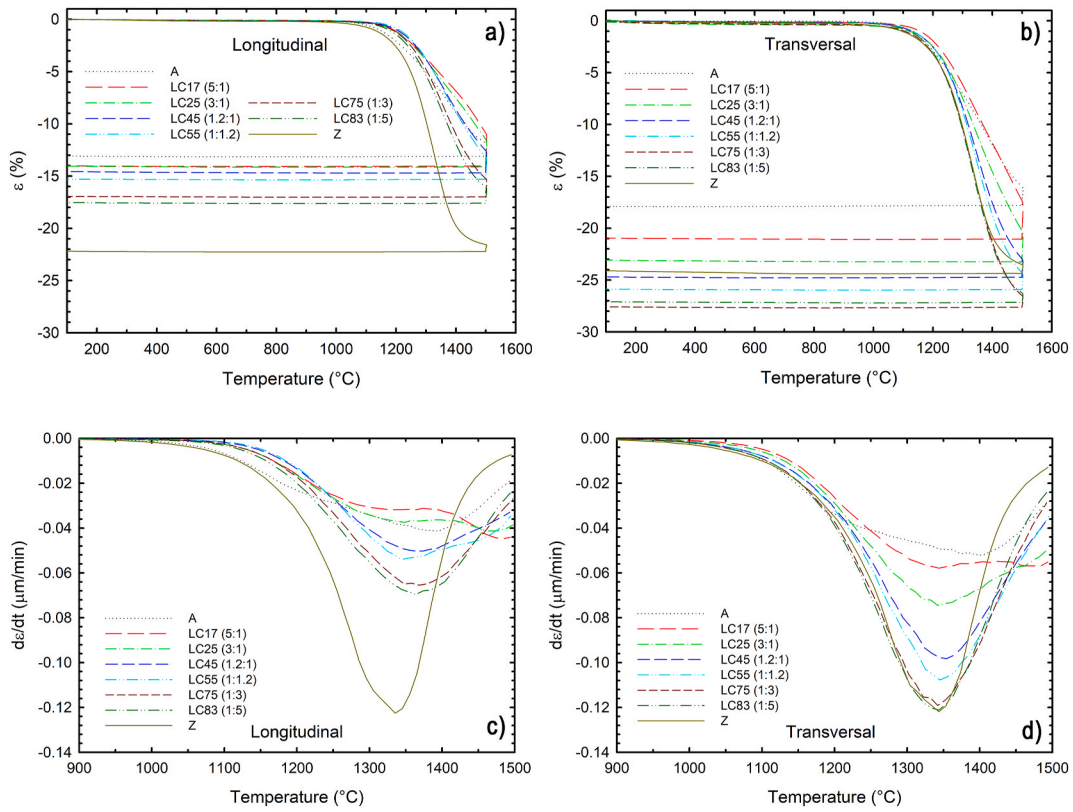

Fig. 5. Sintering shrinkage a, b) and sintering shrinkage rate c, d) of monoliths and layered composites in the longitudinal and transversal orientation of the samples. LC – Layered Composite.

decreases with decreasing particle size [49]. Therefore, zirconia layers shrink at lower temperatures (of around 1300 °C for zirconia monolith) with a higher sintering shrinkage rate at a lower sintering shrinkage maximum, as can be seen in Fig. 5c. Together with the fact that alumina does not yet sinter/shrink at this temperature and many interfaces between alumina and zirconia layers exist, zirconia layers can densify in transversal orientation predominantly [50]. As a result of this, a constrained sintering takes place demonstrated by lower sintering shrinkage of zirconia layers in longitudinal orientation than in transversal one.

The sintering shrinkage in transversal orientation was even higher for most of the layered composites than for zirconia monolith (see Fig. 5b). To explain this abnormality, relative volume change was calculated for pure materials and layered composites (see Fig. 6). As expected, the volume shrinkage gradually increases with increasing zirconia content. It means, that high shrinkage in transversal orientation only compensates for the shrinkage deceleration in the longitudinal orientation and the effect is more pronounced with increasing zirconia content. In pure zirconia, of course, this „compensation“ does not occur.

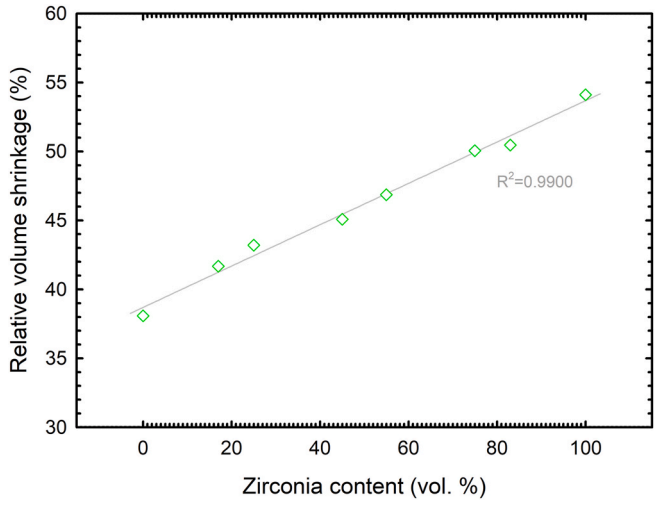

Fig. 6. Dependence of relative volume shrinkage on zirconia content in layered composites.

When comparing Fig. 5c and d, the sintering shrinkage curves in longitudinal orientation show a shift of the maximal shrinkage rate values of layered composites with increasing alumina content to higher temperature into the area appropriate for alumina sintering (around 1400 °C). However, the sintering shrinkage rates of layered composites measured in transversal orientation are similar or close to the sintering shrinkage rate of zirconia monolith. In summary, from the analysis of the sintering shrinkage curves in Fig. 5c and d it emerged that sintering shrinkage of laminates was constrained in the longitudinal direction by alumina which was densified at higher temperatures than zirconia. As a consequence, sintering shrinkage in the transversal direction was accelerated by the preferential shrinkage of zirconia in this direction.

The sintering shrinkage and sintering shrinkage rates of monoliths and particle composites are given in Fig. 7. The samples were measured in longitudinal orientation only. The sintering shrinkage of particle composites was the superposition of the alumina and zirconia shrinkages. Surprisingly, the maximal shrinkage rate occurred at a temperature close to 1500 °C in the particle composite with the lowest zirconia volume fraction, see Fig. 7b. It means, that the sintering was retarded due to the microstructural events discussed below. However, as the volume of zirconia grains in the samples increased, the curves of the shrinkage rate shifted to lower temperatures towards the curve of the zirconia monolith.

Fig. 8 shows the sintering activation energies of monoliths, layered composites in longitudinal and transversal orientations and particle composites. The activation energies were calculated from the Master

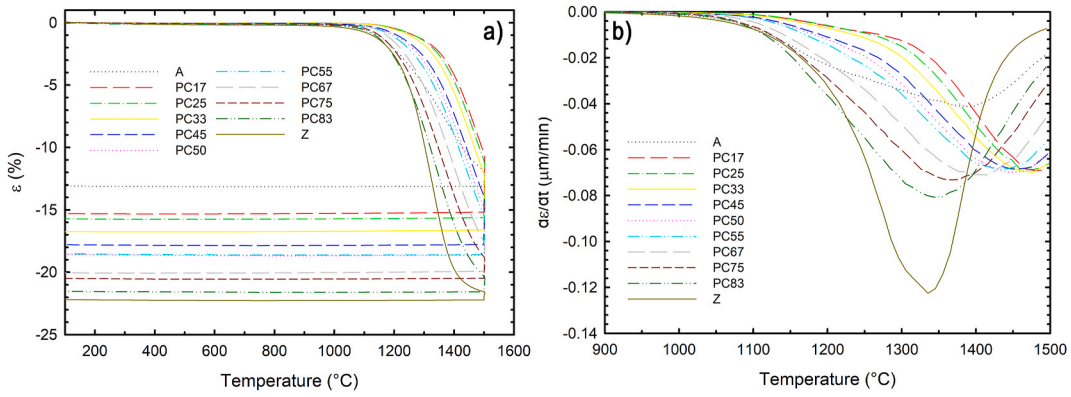

Fig. 7. Sintering shrinkage a) and sintering shrinkage rate b) of monoliths and particle composites. PC – Particle Composite.

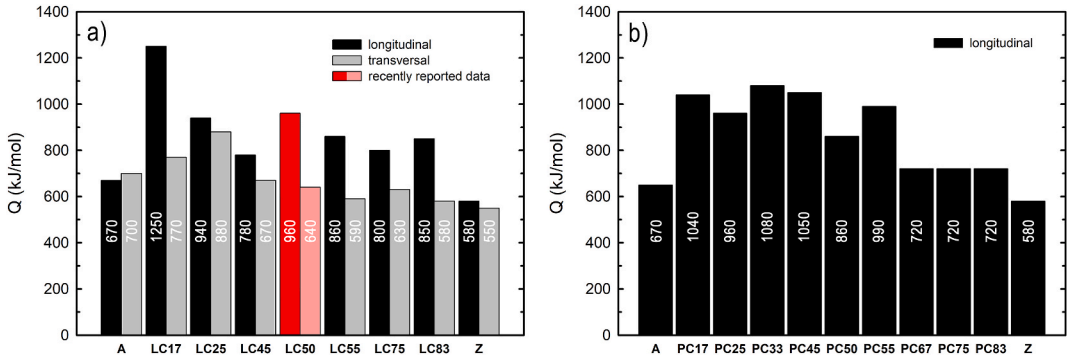

Fig. 8. Sintering activation energies of monoliths, a) layered composites in longitudinal and transversal orientations and b) particle composites (red columns – reported data from Maca et al. [9]). LC – Layered Composite, PC – Particle Composite. (For interpretation of the references to colour in this figure legend, the reader is referred to the Web version of this article.)

Shrinkage Curve model using samples sintered with heating rates of 2, 5, 10, and 20 °C/min in longitudinal as well as in transversal orientations allowing construction of Master Shrinkage Curves given in Fig. 9. Fig. 9 shows a typical example of the layered sample (LC45) having good overlap of individual curves and the MPCD criterion exhibits a single sharp minimum.

It was found that activation energies of alumina and zirconia were 670 and 580 kJ/mol in longitudinal orientation and 700 and 550 kJ/mol in transversal orientation, respectively. These values fit the previously reported data in the literature covering a big scatter in the range of 342–1163 kJ/mol for alumina [1–4,7–13,21,22,51] and 310–990 kJ/mol for zirconia [3,9,14–16,22,52]. The broad values spread is given by evaluation method, morphology [7] and purity of the powder used, considered density interval [14,53,54], different microstructure before sintering and temperature range [9]. In the case of layered composites, the activation energies were always higher than for monoliths due to constrained sintering [55]. The highest activation energies were found for samples with higher alumina content. For longitudinally oriented samples the highest sintering activation energy of 1250 kJ/mol was obtained for the sample with 17 vol% of zirconia, for transversely oriented one it was for the sample with 25 vol% of zirconia (880 kJ/mol). It is also evident that the absolute values of the activation energies were lower in transversal orientation because of the preferential sintering of zirconia.

The activation energies of the particle composites showed a similar trend to that observed for layered ceramics. At low zirconia content, the densification of alumina is slowed down by the so-called pinning effect. It is manifested by an increase in activation energy related to reduced shrinkage rate and the shift of the sintering temperature to higher values (see Fig. 7b). Even at higher zirconia concentrations, the activation energy remains relatively high probably because of the slightly retarded diffusion of atoms in the two-phase material during sintering. The newly obtained results significantly modify the data reported by Wang and Raj [3], who established an activation energy of about 700 kJ/mol for the entire concentration range for this type of particle composite.

Fig. 10 shows typical microstructures of layered and particle composites. Generally, the layered structures can be divided into two groups regarding the strength of the interfaces between layers. The first one is layered structures with weak interfaces findable also in nature (e.g., tooth enamel and sea shells [56]) overcoming their inherent brittleness at static or dynamic loads by deflection or delamination of the propagating crack to generate toughening mechanisms [57,58]. The second group resists against crack propagation by energy-dissipating mechanisms such as crack deflection or bifurcation phenomena due to the presence of compressive residual stresses whose intensity is given by the thickness of layers [59,60]. These layered structures, typically composed of alumina and zirconia [59–62], have strongly bonded interfaces.

Fig. 10a-d shows layered composites with different layer thickness ratios. The EPD allowed to fabrication of multilayer ceramics with sharp, narrow, defect-free and strongly bonded interfaces. However, a certain level of porosity was observed in layered composites, see Table 1, that decreased with zirconia volume. The typical microstructures of the alumina and zirconia individual layers in a layered composite are shown in Fig. 11. Some porosity is evident in alumina while the zirconia layer is fully dense which corresponds with the density measurements of monoliths. Therefore, the density in layered composites depends on the thickness of the alumina layers (alumina volume) in particular.

The second benefit of the fabrication method is nicely dispersed alumina and zirconia grains in the sintered microstructures of the particle composites, as demonstrated in Fig. 10e-h. The mean grain size of the particle as well as layered composites is shown in Fig. 12. The graph

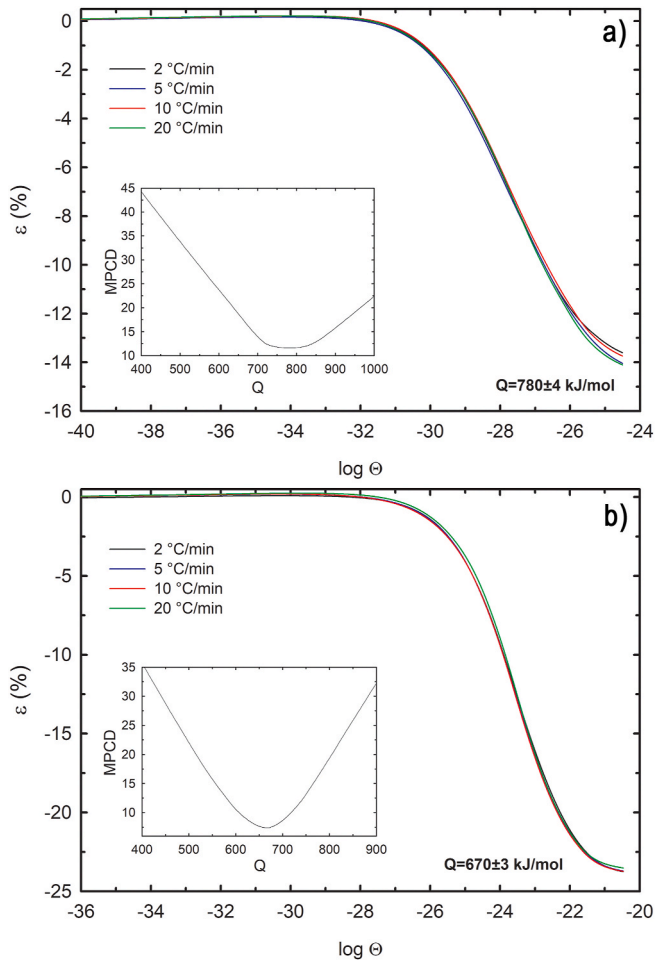

Fig. 9. Master Shrinkage Curves of LC45 sample in longitudinal and transversal orientations.

shows the usefulness of adding a dispersed second phase to control grain growth during sintering. The MGS of alumina in particle composites decreased at low zirconia contents as a consequence of the pinning effect [55]. Subsequently, the MGS size was mainly affected by retarded diffusion caused by an increasing zirconia concentration. On the other

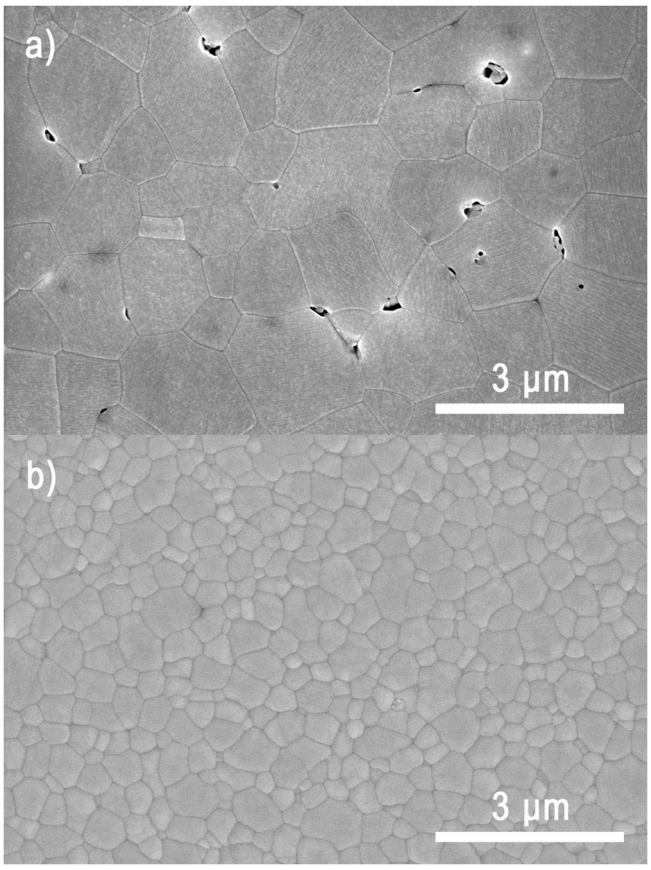

Fig. 11. Microstructures of a) alumina layer and b) zirconia layer in the layered composite LC75.

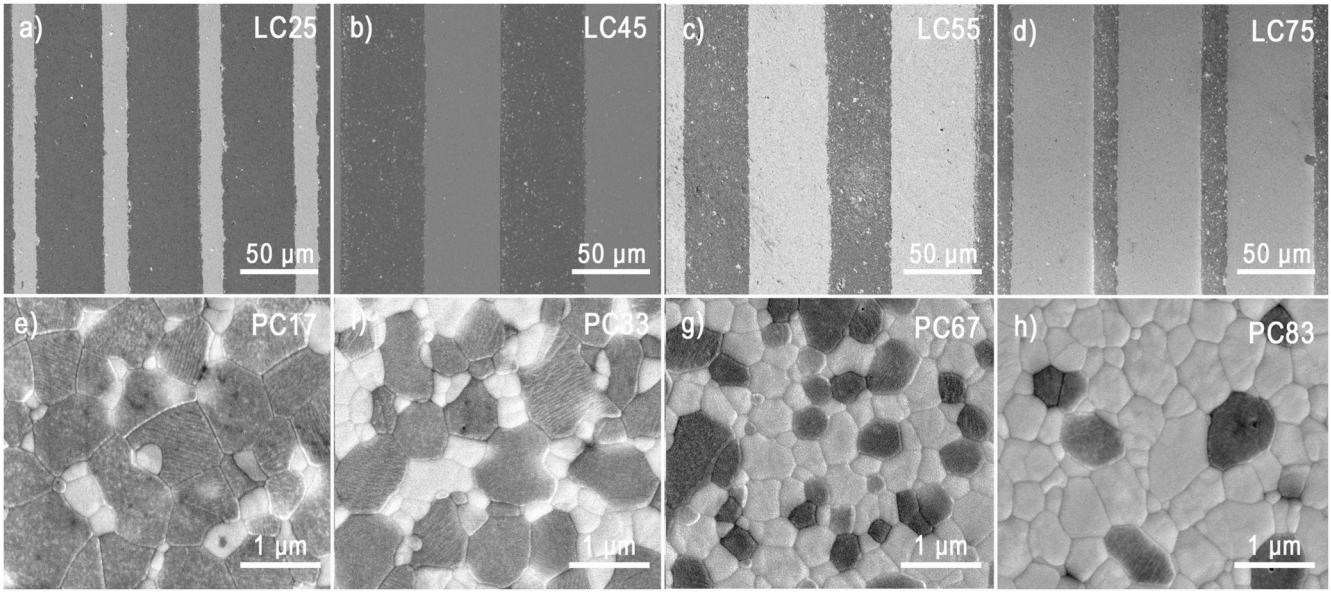

Fig. 10. Micrographs a-d) layered and e-h) particle composite microstructures (alumina – dark fields, zirconia – bright fields). LC – Layered Composite, PC – Particle Composite.

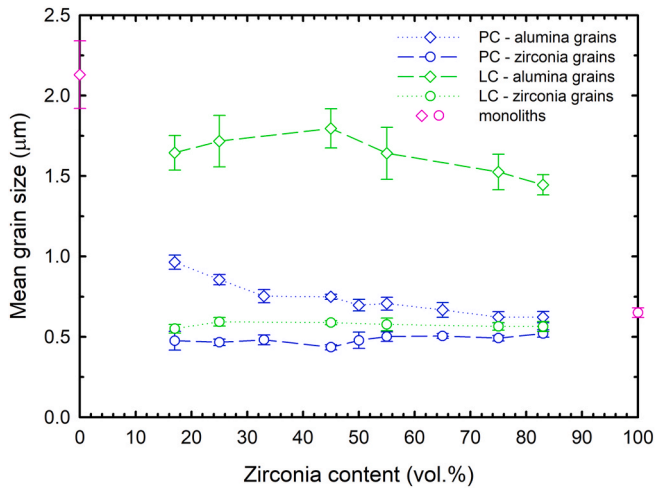

Fig. 12. Dependence of mean grain size on zirconia content in monoliths, layered and particle composites (in longitudinal orientation) sintered at 1500 °C for 2 h with a heating rate of 10 °C/min (pink symbols – reported data from Maca et al. [9]). LC – Layered Composite, PC – Particle Composite. (For interpretation of the references to colour in this figure legend, the reader is referred to the Web version of this article.)

hand, the MGS of zirconia remained unaffected in particle composite microstructures because it is widely believed that alumina grains effectively impede the mobility of zirconia grain boundaries in Alumina Toughened Zirconia composites [63]. Approximately 50 vol% of alumina in the microstructure seems to be beneficial for stabilising MGS on the minimal level possible. However, a higher volume of alumina in the composite resulted in lower density, see Table 1. As a confirmation of this, certain porosity is present in the microstructures in Fig. 10e and f. Contrary, two distinct populations of MGSs were measured in layered composites. There is no reason for pinning effect application in alumina or zirconia layers behaving more as monolithic ceramics, so their grain growth is driven by original particle size, chemical nature, packing density, and sintering temperature.

The mechanical properties of laminates according to their layer design and total volume fraction of phases are in the literature well described [43,62,64]. The apparent fracture toughness and flexural strength depend on the developed internal stresses (see Fig. 3a) due to CTE mismatch given by alumina-zirconia laminate prepared by EPD similar to the laminate used in this work [39,44]. The laminate prepared for this study contains a higher number of layers which is not optimal for the strength and fracture toughness [43]. The crack behaviour during indentation for laminates was clearly described here [65] showing that the indentation method is not suitable to characterize fracture behaviour when internal stresses are present.

However, Vickers hardness and indentation elastic modulus development with increasing addition of zirconia to the alumina matrix determined for particle composite can provide valuable information. The dependencies are shown in Fig. 13 where average values together with indicated standard deviation by error bars are plotted. The general trend is obvious that with increasing amounts of zirconia, both hardness and elastic modulus decreases.

When a single-phase material is loaded, the corresponding deformation is uniformly distributed over the whole body. In a material composed of two phases, the deformation is distributed between the phases according to their stiffness. A standard method used for estimating the overall mechanical properties of a composite material is based on the rule of mixtures (RoM). The simplest linear combination of the Vickers hardness HV (or elastic modulus E) versus the volume fraction of the phases is given by the iso-stress model (Voigt) [66]:

$$HV_c = HV_f \bullet v_f + HV_m \bullet \left(1 - v_f\right), or\ E_c = E_f \bullet v_f + E_m \bullet \left(1 - v_f\right) \quad (9)$$

where v_f is the reinforcement volume fraction, HV_m and HV_f are the Vickers hardness and E_m, E_f is the elastic modulus of the matrix and reinforcement, respectively. The Voigt model originates from the axial loading of continuous fibre-reinforced composites. When materials with large differences in hardness are combined, it is clear that the deformation of the soft matrix is greater than that of the hard particles. On the other hand, the deformation of the hard matrix containing soft particles increases and the hardness can be lower than predicted by Eq. (9). In these cases, to estimate the Vickers hardness HV (or elastic modulus E), Reuss proposed the iso-strain model as a lower bound of the RoM method [66]:

$$HV_c = \left(\frac{v_f}{HV_f} + \frac{\left(1 - v_f\right)}{HV_m}\right)^{-1}, or\ E_c = \left(\frac{v_f}{E_f} + \frac{\left(1 - v_f\right)}{E_m}\right)^{-1}. \quad (10)$$

The predictions of the Vickers hardness HV and indentation elastic modulus E_{IT} of the fabricated particle composites based on Eq. (9) and Eq. (10) are given in Fig. 13 by the dashed lines. The indentation elastic modulus keeps the trend given by the mixture law (Eq. (9)) given by input values of pure alumina and zirconia as can be seen in Fig. 13. In contrast, the Vickers hardness of the prepared particle composites significantly differs from the predictions given by the RoM methods. The observed change in Vickers hardness of the prepared particle composites is influenced by several jointly acting effects such as interconnection of phases, internal thermal stresses present, transformation toughening by zirconia and grain size pinning effect.

The main effect can be attributed to the developed internal stresses. According to the literature, experimental data lay mostly close to the zirconia matrix inclusion bounds (see Fig. 3b) - full line) even for higher concentrations of reinforcement (i.e. forming continuous phase) [46,67,

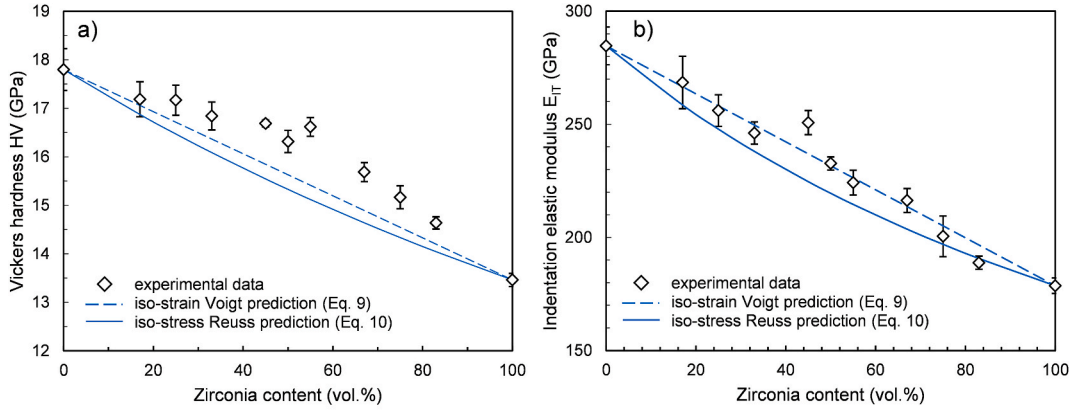

Fig. 13. Dependence of a) Vickers hardness HV and b) indentation elastic modulus E_{IT} on zirconia content in the particle composites.

68]. This influence can be affected by the development of additional stresses caused by volume change during the stress-induced transformation of partially stabilised tetragonal zirconia grains during loading [25,69–72]. This effect can be weakened by spontaneous transformation due to the development of internal stresses during cooling from sintering temperature [72].

Interconnectivity and gain pinning effect are other factors influencing mechanical behaviour. The isolated grains of the secondary (reinforcing) phase are restricted in their growth due to a lack of material in the surrounding eliminating diffusion processes during sintering. On the other hand, the grains in the matrix are also restricted in the grain growth by the pinning effect [73]. Therefore, the development of grain size distributions for both phases is very dependent except the volume fraction also on the processing conditions (temperature, dwell time etc.) and the initial particle size and level of dispersion of the reinforcing phase. The development of the grain size for all composites under investigation is shown in Fig. 12. Some relations can be found between the restricted gain growth and activation energies determined during sintering, see Fig. 8.

Generally, the formation of continuous phase from one of two phases of the same grain size should change symmetrically with the threshold depending on the theory used. In our particle composite is the situation more complex because the particle/grain sizes are different for each phase and each composition because of geometrical and physical reasons. The breakpoint will be shifted from the equilibrium of 50 vol % to between 55 and 67 %. This fact corresponds well to the hardness development shown in Fig. 13 where two different trends (slopes) depending on the composition can be observed. The first slope can be seen for 0–55 % of zirconia and the second one is steeper from 67 % to 100 % of zirconia. We believe that the dominance of the interconnected phase is responsible for this behaviour. The enhanced hardness values (above the RoM upper bound) can be explained by the synergism of developed internal stresses, transformation toughening, and formation of interconnected phases and therefore the number of biphase interfaces [74].

Contrary to hardness, the indentation elastic modulus keeps the trend given by the RoM given by values of alumina and zirconia as can be seen in Fig. 13. Also, here is an effect of relative densities (shown in Table 1) mirrored to the scattering of values and slight differences from the linear dependence. The effect of the interconnected phase is not observable as in the case of Vickers hardness because the level of internal stresses and grain size does not change elastic modulus.

Summing all together the above-mentioned effects acting and affecting the mechanical properties can be concluded that there is no direct relationship between the activation energy of sintering. The only relationship through the resulting microstructure and amount of biphase interfaces can be found. The number of interfaces is higher for the particle composite than in the case of laminates having the same volume fraction. Also, the grain size pinning effect is more pronounced in particle composites because in laminates the majority of grains within one phase are interconnected.

4. Conclusions

The complex evaluation of particulate and laminate composites by the modified Master Sintering Curve concept was done for the whole range of compositions for the first time. The alumina/zirconia composites designed as layers in various thickness ratios or dispersed particles covering the entire concentration profile were successfully prepared using electrophoretic deposition (EPD). The composites with strongly bounded interfaces were obtained.

Sintering of the composites was monitored by high-temperature dilatometry in the longitudinal and transversal orientation of the samples. The pure alumina and zirconia monoliths showed shrinkage anisotropy due to the morphology of starting ceramic particles. In the case of layered composites, the sintering in longitudinal orientation was more controlled by the alumina than zirconia content resulting in constrained sintering. On the other hand, in the transversal orientation, the shrinkage only compensates for the shrinkage deceleration in the longitudinal orientation. The effect was more pronounced with increasing zirconia content. Therefore, the sintering shrinkage in transversal orientation was even higher for most layered composites than for zirconia monolith. The sintering shrinkage of particle composites was the superposition of the alumina and zirconia shrinkages.

Sintering activation energies of layered composites were always higher than for monoliths due to constrained sintering. However, the absolute values of the activation energies were lower in transversal orientation because of the preferential sintering of zirconia. In both orientations, the highest sintering activation energies were calculated for samples with lower content of zirconia, i.e. 17 vol% (1250 kJ/mol - transversal orientation) and 25 vol% (880 kJ/mol - transversal orientation). In the case of particle composites, the increase of sintering activation energy (~1100 kJ/mol) at low zirconia content was attributed to the slowed-down densification of alumina by the pinning effect caused by smaller zirconia particles. These results significantly modify reported knowledge to date.

The microstructural analysis showed that EPD allowed to fabrication of multilayer ceramics with sharp, narrow, defect-free and strongly bonded interfaces and particle composites with nicely dispersed alumina and zirconia grains in the sintered microstructures. Moreover, in the particle composites, the mean grain size of alumina decreased at low zirconia contents confirming the pinning effect.

The mechanical properties represented by Vickers hardness measured for particle composite varied from the theoretical predictions, especially for the compositions exhibiting the highest activation energies, however, no direct relationship between the hardness and activation energy was found. The observed behaviour was interpreted with the help of microstructural interconnectivity between phases given by initial particle size, development of internal stresses during cooling down from the sintering temperature and grain size pinning effect. Contrary to the hardness the indentation elastic modulus respects well the upper bound of the rule of mixture given by Voigt's iso-stress model.

CRediT authorship contribution statement

Daniel Drdlik: Conceptualization, Formal analysis, Investigation, Methodology, Writing – original draft. **Ilya Sokolov:** Formal analysis, Investigation. **Hynek Hadraba:** Formal analysis, Investigation, Writing – review & editing. **Zdenek Chlup:** Investigation, Methodology, Writing – original draft, Formal analysis. **Katarina Drdlikova:** Writing – review & editing. **Karel Maca:** Conceptualization, Validation, Writing – review & editing.

Declaration of competing interest

The authors declare that they have no known competing financial interests or personal relationships that could have appeared to influence the work reported in this paper.

Acknowledgements

This publication was supported by the project "Mechanical Engineering of Biological and Bio-inspired Systems", funded as project No. CZ.02.01.01/00/22_008/0004634 by Programme Johannes Amos Commenius, call Excellent Research. We acknowledge CzechNanoLab Research Infrastructure supported by MEYS CR (LM2023051) and Brno University of Technology for grant No. FSI–S-23-8226.

References

[1] W.S. Young, I.B. Cutler, Initial sintering with constant rates of heating, J. Am. Ceram. Soc. 53 (1970) 659–663, https://doi.org/10.1111/j.1151-2916.1970.tb12036.x.

[2] J. Wang, R. Raj, Estimate of the activation energies for boundary diffusion from rate-controlled sintering of pure alumina, and alumina doped with zirconia or titania, J. Am. Ceram. Soc. 73 (1990) 1172–1175, https://doi.org/10.1111/j.1151-2916.1990.tb05175.x.

[3] J. Wang, R. Raj, Activation energy for the sintering of two-phase alumina/zirconia ceramics, J. Am. Ceram. Soc. 74 (1991) 1959–1963, https://doi.org/10.1111/j.1151-2916.1991.tb07815.x.

[4] H.H. Su, D.L. Johnson, Master sintering curve: a practical approach to sintering, J. Am. Ceram. Soc. 79 (1996) 3211–3217, https://doi.org/10.1111/j.1151-2916.1996.tb08097.x.

[5] M.H. Teng, Y.C. Lai, Y.T. Chen, A computer program of master sintering curve model to accurately predict sintering results, West. Pac. Earth Sci. 2 (2002) 171–180.

[6] D.C. Blaine, S.-J. Park, R.M. German, Linearization of master sintering curve, J. Am. Ceram. Soc. 92 (2009) 1403–1409, https://doi.org/10.1111/j.1551-2916.2009.03011.x.

[7] V. Pouchly, K. Maca, Master sintering curve: a practical approach to its construction, Sci. Sinter. 42 (2010) 25–32, https://doi.org/10.2298/SOS1001025P.

[8] F. Zuo, A. Badev, S. Saunier, D. Goeuriot, R. Heuguet, S. Marinel, Microwave versus conventional sintering: estimate of the apparent activation energy for densification of α-alumina and zinc oxide, J. Eur. Ceram. Soc. 34 (2014) 3103–3110, https://doi.org/10.1016/j.jeurceramsoc.2014.04.006.

[9] K. Maca, V. Pouchly, D. Drdlik, H. Hadraba, Z. Chlup, Dilatometric study of anisotropic sintering of alumina/zirconia laminates with controlled fracture behaviour, J. Eur. Ceram. Soc. 37 (2017) 4287–4295, https://doi.org/10.1016/j.jeurceramsoc.2017.04.030.

[10] Z. He, J. Ma, Densification and grain growth during interface reaction controlled sintering of alumina ceramics, Ceram. Int. 27 (2001) 261–264, https://doi.org/10.1016/S0272-8842(00)00073-0.

[11] W.Q. Shao, S.O. Chen, D. Li, H.S. Cao, Y.C. Zhang, S.S. Zhang, Prediction of densification and microstructure evolution for α-Al_2O_3 during pressureless sintering at low heating rates based on the master sintering curve theory, Sci. Sinter. 40 (2008) 251–261, https://doi.org/10.2298/SOS0803251S.

[12] M. Aminzare, M. Mazaheri, F. Golestani-fard, H.R. Rezaie, R. Ajeian, Sintering behavior of nano alumina powder shaped by pressure filtration, Ceram. Int. 37 (2011) 9–14, https://doi.org/10.1016/j.ceramint.2010.07.027.

[13] T.-T. Fang, J.-T. Shiue, F.-S. Shiau, On the evaluation of the activation energy of sintering, Mater. Chem. Phys. 80 (2003) 108–113, https://doi.org/10.1016/S0254-0584(02)00373-5.

[14] G. Bernard-Granger, C. Guizard, Apparent activation energy for the densification of a commercially available granulated zirconia powder, J. Am. Ceram. Soc. 90 (2007) 1246–1250, https://doi.org/10.1111/j.1551-2916.2006.01415.x.

[15] R.F. Marcomini, V.L. Arantes, Sintering mechanisms of partially stabilized zirconia (TZ3Y) with ZnO and Co_3O_4 as sintering additives, Cerâmica 67 (2021) 244–249, https://doi.org/10.1590/0366-69132021673823099.

[16] K. Matsui, N. Ohmichi, M. Ohgai, N. Enomoto, J. Hojo, Sintering kinetics at constant rates of heating: effect of Al_2O_3 on the initial sintering stage of fine zirconia powder, J. Am. Ceram. Soc. 88 (2005) 3346–3352, https://doi.org/10.1111/j.1551-2916.2005.00620.x.

[17] C.C. Ye, W.Q. Wei, X. Fu, C.H. Wang, H.Q. Ru, Effect of sintering activation energy on Si_3N_4 composite ceramics, Ceram. Int. 48 (2022) 4851–4857, https://doi.org/10.1016/j.ceramint.2021.11.021.

[18] P. Dehaudt, L. Bourgeois, H. Chevrel, Activation energy of UO_2 and UO_{2+x} sintering, J. Nucl. Mater. 299 (2001) 250–259, https://doi.org/10.1016/S0022-3115(01)00661-4.

[19] D. Lahiri, S.V.R. Rao, G.V.S.H. Rao, R.K. Srivastava, Study on sintering kinetics and activation energy of UO_2 pellets using three different methods, J. Nucl. Mater. 357 (2006) 88–96, https://doi.org/10.1016/j.jnucmat.2006.05.046.

[20] K. Nakajima, R.H.R. Castro, Thermodynamics and kinetics of sintering of Y_2O_3, J. Am. Ceram. Soc. 103 (2020) 4903–4912, https://doi.org/10.1111/jace.17273.

[21] H. Su, D.L. Johnson, Sintering of alumina in microwave-induced oxygen plasma, J. Am. Ceram. Soc. 79 (1996) 3199–3210, https://doi.org/10.1111/j.1151-2916.1996.tb08096.x.

[22] V. Pouchly, K. Maca, Y. Xiong, J.Z. Shen, Master Sintering Surface – a practical approach to its construction and utilization for spark plasma sintering prediction, Sci. Sinter. 44 (2012) 169–175, https://doi.org/10.2298/SOS1202169P.

[23] A. Okada, Automotive and industrial applications of structural ceramics in Japan, J. Eur. Ceram. Soc. 28 (2008) 1097–1104, https://doi.org/10.1016/j.jeurceramsoc.2007.09.016.

[24] S.R. Banik, I.M. Iqbal, R. Nath, L.J. Bora, B.K. Singh, N. Mandal, M.R. Sankar, State of the art on zirconia toughened alumina cutting tools, Mater. Today: Proc. 18 (2019) 2632–2641, https://doi.org/10.1016/j.matpr.2019.07.123.

[25] M.M. Basha, S.M. Basha, B.K. Singh, N. Mandal, M.R. Sankar, A review on synthesis of zirconia toughened alumina (ZTA) for cutting tool applications, Mater. Today: Proc. 26 (2020) 534–541, https://doi.org/10.1016/j.matpr.2019.12.134.

[26] T.E. Steyer, Shaping the future of ceramics for aerospace applications, Int. J. Appl. Ceram. Technol. 10 (2013) 389–394, https://doi.org/10.1111/ijac.12069.

[27] E. Yousefi, M. Adineh, M.B. Askari, An investigation on microstructural and mechanical properties of porous zirconia-alumina nanocomposite prepared by solid state sintering method, Anti-Corros, Methods Mater 65 (2018) 138–145, https://doi.org/10.1108/ACMM-03-2017-1773.

[28] J. Lalande, S. Scheppokat, R. Janssen, N. Claussen, Toughening of alumina/zirconia ceramic composites with silver particles, J. Eur. Ceram. Soc. 22 (2002) 2165–2171, https://doi.org/10.1016/S0955-2219(02)00031-6.

[29] G. Schierano, F. Mussano, M.G. Faga, G. Menicucci, C. Manzella, C. Sabione, T. Genova, M.M.v. Degerfeld, B. Peirone, A. Cassenti, P. Cassoni, S. Carossa, An alumina toughened zirconia composite for dental implant application: in vivo animal results, BioMed Res. Int. 2015 (2015) 157360, https://doi.org/10.1155/2015/157360.

[30] F. Mussano, T. Genova, L. Munaron, M.G. Faga, S. Carossa, Ceramic biomaterials for dental implants: current use and future perspectives, in: A. Mazen Ahmad Jawad Amin (Ed.), Dental Implantology and Biomaterial, IntechOpen, Rijeka, 2016. Ch. 4.

[31] S. Sequeira, M.H. Fernandes, N. Neves, M.M. Almeida, Development and characterization of zirconia–alumina composites for orthopedic implants, Ceram. Int. 43 (2017) 693–703, https://doi.org/10.1016/j.ceramint.2016.09.216.

[32] S.M. Kurtz, S. Kocagöz, C. Arnholt, R. Huet, M. Ueno, W.L. Walter, Advances in zirconia toughened alumina biomaterials for total joint replacement, J. Mech. Behav. Biomed. Mater. 31 (2014) 107–116, https://doi.org/10.1016/j.jmbbm.2013.03.022.

[33] B.J. McEntire, B.S. Bal, M.N. Rahaman, J. Chevalier, G. Pezzotti, Ceramics and ceramic coatings in orthopaedics, J. Eur. Ceram. Soc. 35 (2015) 4327–4369, https://doi.org/10.1016/j.jeurceramsoc.2015.07.034.

[34] D.J. Green, P.Z. Cai, G.L. Messing, Residual stresses in alumina–zirconia laminates, J. Eur. Ceram. Soc. 19 (1999) 2511–2517, https://doi.org/10.1016/S0955-2219(99)00103-X.

[35] Z. Chlup, H. Hadraba, D. Drdlik, K. Maca, I. Dlouhy, R. Bermejo, On the determination of the stress-free temperature for alumina–zirconia multilayer structures, Ceram. Int. 40 (2014) 5787–5793, https://doi.org/10.1016/j.ceramint.2013.11.018.

[36] H. Moon, M.G. Pontin, F.F. Lange, Crack interactions in laminar ceramics that exhibit a threshold strength, J. Am. Ceram. Soc. 87 (2004) 1694–1700, https://doi.org/10.1111/j.1551-2916.2004.01694.x.

[37] J. Gurauskis, A.J. Sánchez-Herencia, C. Baudín, Alumina–zirconia layered ceramics fabricated by stacking water processed green ceramic tapes, J. Eur. Ceram. Soc. 27 (2007) 1389–1394, https://doi.org/10.1016/j.jeurceramsoc.2006.04.081.

[38] H. Hadraba, D. Drdlik, Z. Chlup, K. Maca, I. Dlouhy, Control of electrophoretic deposition kinetics for preparation of laminated alumina/zirconia ceramic composites, Key Eng. Mater. 507 (2012) 209–213, https://doi.org/10.4028/www.scientific.net/KEM.507.209.

[39] H. Hadraba, D. Drdlik, Z. Chlup, K. Maca, I. Dlouhy, J. Cihlar, Layered ceramic composites via control of electrophoretic deposition kinetics, J. Eur. Ceram. Soc. 33 (2013) 2305–2312, https://doi.org/10.1016/j.jeurceramsoc.2013.01.026.

[40] J.D. Hansen, R.P. Rusin, M.-H. Teng, D.L. Johnson, Combined-stage sintering model, J. Am. Ceram. Soc. 75 (1992) 1129–1135, https://doi.org/10.1111/j.1151-2916.1992.tb05549.x.

[41] K.J. An, M.K. Han, H.J. Kim, The pressure-assisted master sintering surface of metallic powder mixture, Mater. Trans. 51 (2010) 822–825, https://doi.org/10.2320/matertrans.M2009303.

[42] M.I. Mendelson, Average grain size in polycrystalline ceramics, J. Am. Ceram. Soc. 52 (1969) 443–446, https://doi.org/10.1111/j.1151-2916.1969.tb11975.x.

[43] L. Sestakova, R. Bermejo, Z. Chlup, R. Danzer, Strategies for fracture toughness, strength and reliability optimisation of ceramic-ceramic laminates, Int. J. Mater. Res. 102 (2011) 613–626. https://doi:10.3139/146.110523.

[44] Z. Chlup, H. Hadraba, L. Slabáková, D. Drdlik, I. Dlouhy, Fracture behaviour of alumina and zirconia thin layered laminate, J. Eur. Ceram. Soc. 32 (2012) 2057–2061, https://doi.org/10.1016/j.jeurceramsoc.2011.09.006.

[45] J.D. Eshelby, The determination of the elastic field of an ellipsoidal inclusion, and related problems, Proc. R. Soc. A: Math. Phys. Eng. Sci. 241 (1957) 376–396, https://doi.org/10.1098/rspa.1957.0133.

[46] Y. Akiniwa, K. Tanaka, N. Minakawa, Y. Morii, Neutron diffraction study of thermal residual stress in ceramic composite, J. Soc. Mater. Sci. Jap. 49 (2000) 281–286, https://doi.org/10.2472/jsms.49.12Appendix_281.

[47] D. Drdlik, I. Sokolov, H. Hadraba, Z. Chlup, K. Drdlikova, K. Maca, Data for "Sintering activation energies of anisotropic layered and particle alumina/zirconia-based composites and their mechanical response", Zenodo, v1, 2024, https://doi.org/10.5281/zenodo.10592589.

[48] S. Yang, W. Cai, G. Liu, H. Zeng, From nanoparticles to nanoplates: preferential oriented connection of Ag colloids during electrophoretic deposition, J. Phys. Chem. C 113 (2009) 7692–7696, https://doi.org/10.1021/jp901961h.

[49] M.J. Mayo, Processing of nanocrystalline ceramics from ultrafine particles, Int. Mater. Rev. 41 (1996) 85–115, https://doi.org/10.1179/imr.1996.41.3.85.

[50] A.J. Sánchez-Herencia, J. Gurauskis, C. Baudín, Processing of Al_2O_3/Y-TZP laminates from water-based cast tapes, Compos. B Eng. 37 (2006) 499–508, https://doi.org/10.1016/j.compositesb.2006.02.002.

[51] B. Baruah, R. Anand, S.K. Behera, Master sintering curve and activation energy of sintering of ZrO_2-doped Al_2O_3, Ceram. Int. 47 (2021) 7253–7257, https://doi.org/10.1016/j.ceramint.2020.11.001.

[52] A.J. Rayner, R.M.C. Clemmer, S.F. Corbin, Determination of the activation energy and master sintering curve for NiO/YSZ composite solid oxide fuel cell anodes, J. Am. Ceram. Soc. 98 (2015) 1060–1065, https://doi.org/10.1111/jace.13405.

[53] V. Pouchly, K. Maca, Z. Shen, Two-stage master sintering curve applied to two-step sintering of oxide ceramics, J. Eur. Ceram. Soc. 33 (2013) 2275–2283, https://doi.org/10.1016/j.jeurceramsoc.2013.01.020.

[54] K. Maca, V. Pouchlý, K. Bodišová, P. Švančárek, D. Galusek, Densification of fine-grained alumina ceramics doped by magnesia, yttria and zirconia evaluated by two different sintering models, J. Eur. Ceram. Soc. 34 (2014) 4363–4372, https://doi.org/10.1016/j.jeurceramsoc.2014.06.030.
[55] F.F. Lange, M.M. Hirlinger, Hindrance of grain growth in Al_2O_3 by ZrO_2 inclusions, J. Am. Ceram. Soc. 67 (1984) 164–168, https://doi.org/10.1111/j.1151-2916.1984.tb19734.x.
[56] M.A. Meyers, P.-Y. Chen, A.Y.-M. Lin, Y. Seki, Biological materials: structure and mechanical properties, Prog. Mater. Sci. 53 (2008) 1–206, https://doi.org/10.1016/j.pmatsci.2007.05.002.
[57] H. Tomaszewski, H. Węglarz, A. Wajler, M. Boniecki, D. Kalinski, Multilayer ceramic composites with high failure resistance, J. Eur. Ceram. Soc. 27 (2007) 1373–1377, https://doi.org/10.1016/j.jeurceramsoc.2006.04.030.
[58] A. Ceylan, P.A. Fuierer, Fracture toughness of alumina/lanthanum titanate laminate composites with a weak interface, Mater. Lett. 61 (2007) 551–555, https://doi.org/10.1016/j.matlet.2006.05.021.
[59] A.J. Blattner, R. Lakshminarayanan, D.K. Shetty, Toughening of layered ceramic composites with residual surface compression: effects of layer thickness, Eng. Fract. Mech. 68 (2001) 1–7, https://doi.org/10.1016/S0013-7944(00)00096-5.
[60] R. Bermejo, Y. Torres, A.J. Sánchez-Herencia, C. Baudín, M. Anglada, L. Llanes, Residual stresses, strength and toughness of laminates with different layer thickness ratios, Acta Mater. 54 (2006) 4745–4757, https://doi.org/10.1016/j.actamat.2006.06.008.
[61] R. Lakshminarayanan, D.K. Shetty, R.A. Cutler, Toughening of layered ceramic composites with residual surface compression, J. Am. Ceram. Soc. 79 (1996) 79–87, https://doi.org/10.1111/j.1151-2916.1996.tb07883.x.
[62] R. Bermejo, Y. Torres, C. Baudín, A.J. Sánchez-Herencia, J. Pascual, M. Anglada, L. Llanes, Threshold strength evaluation on an Al_2O_3–ZrO_2 multilayered system, J. Eur. Ceram. Soc. 27 (2007) 1443–1448, https://doi.org/10.1016/j.jeurceramsoc.2006.05.037.
[63] M.K.G. Abbas, S. Ramesh, S.F.H. Tasfy, K.Y.S. Lee, A state-of-the-art review on alumina toughened zirconia ceramic composites, Mater. Today Commun. 37 (2023) 106964, https://doi.org/10.1016/j.mtcomm.2023.106964.
[64] R. Bermejo, Y. Torres, A.J. Sánchez-Herencia, C. Baudín, M. Anglada, L. Llanes, Fracture behaviour of an Al_2O_3–ZrO_2 multi-layered ceramic with residual stresses due to phase transformations, Fatigue Fract. Eng. Mater. Struct. 29 (2006) 71–78, https://doi.org/10.1111/j.1460-2695.2006.00962.x.
[65] Z. Chlup, L. Novotná, F. Šiška, D. Drdlík, H. Hadraba, Effect of residual stresses to the crack path in alumina/zirconia laminates, J. Eur. Ceram. Soc. 40 (2020) 5810–5818, https://doi.org/10.1016/j.jeurceramsoc.2020.06.044.
[66] H.S. Kim, On the rule of mixtures for the hardness of particle reinforced composites, Mater. Sci. Eng. A 289 (2000) 30–33, https://doi.org/10.1016/S0921-5093(00)00909-6.
[67] G. Pezzotti, V. Sergo, O. Sbaizero, N. Muraki, S. Meriani, T. Nishida, Strengthening contribution arising from residual stresses in Al_2O_3/ZrO_2 composites: a piezo-Spectroscopy investigation, J. Eur. Ceram. Soc. 19 (1999) 247–253, https://doi.org/10.1016/S0955-2219(98)00195-2.
[68] Q. Ma, W. Pompe, J.D. French, D.R. Clarke, Residual stresses in Al_2O_3-ZrO_2 composites: a test of stochastic stress models, Acta Metall. Mater. 42 (1994) 1673–1681, https://doi.org/10.1016/0956-7151(94)90377-8.
[69] B. Basu, J. Vleugels, O. Van Der Biest, ZrO_2–Al_2O_3 composites with tailored toughness, J. Alloys Compd. 372 (2004) 278–284, https://doi.org/10.1016/j.jallcom.2003.09.157.
[70] V. Naglieri, P. Palmero, L. Montanaro, J. Chevalier, Elaboration of alumina-zirconia composites: role of the zirconia content on the microstructure and mechanical properties, Materials (2013) 2090–2102.
[71] D. Casellas, M.M. Nagl, L. Llanes, M. Anglada, Fracture toughness of alumina and ZTA ceramics: microstructural coarsening effects, J. Mater. Process. Technol. 143–144 (2003) 148–152, https://doi.org/10.1016/S0924-0136(03)00396-0.
[72] J. Wang, R. Stevens, Zirconia-toughened alumina (ZTA) ceramics, J. Mater. Sci. 24 (1989) 3421–3440, https://doi.org/10.1007/BF02385721.
[73] K. Okada, T. Sakuma, The role of Zener's pinning effect on the grain growth in Al_2O_3-ZrO_2, J. Ceram. Soc. Jap. 100 (1992) 382–386, https://doi.org/10.2109/JCERSJ.100.382.
[74] R.M. German, Particulate Composites, first ed., Springer, Cham, 2016.